# Nonlinear analysis of causality for heat flow in heavy-ion collisions: constraints from equation of state

Victor Roy

School of Physical Sciences, National Institute of Science Education and Research, Bhubaneswar 752050, India. and
Homi Bhabha National Institute, Training School Complex,
Anushaktinagar, Mumbai 400094, Maharashtra, India.

(Dated: August 6, 2025)

We explore the causal parameter space of the Mueller-Israel-Stewart second-order theory for heat-conducting fluids in nonlinear regimes for one-dimensional fluid flow. We show that this parameter space is highly constrained and particularly sensitive to the equation of state and second-order transport coefficients. Through numerical analysis of the characteristic equations, we identify regions of strong hyperbolicity, weak hyperbolicity, and non-hyperbolicity, mapping the boundaries of causality violation as functions of the heat flux to energy density ratio  $q/\varepsilon$  and relaxation parameters. We also explore the causality conditions using a realistic lattice QCD-based equation of state. Using the Navier-Stokes approximation, we estimate the heat flow magnitude to assess causality criteria for one-dimensional heat conduction in heavy-ion collisions. Our calculations reveal unrealistically large heat flux values ( $|\mathbf{q}|/\varepsilon \sim 330-811$ ) for typical RHIC conditions when using thermal conductivity estimates from kinetic theory models, suggesting either significant overestimation of transport coefficients or breakdown of the fluid approximation in these extreme conditions. The pressure gradient corrections reduce the heat flow by approximately 15% but do not resolve the causality concerns.

## I. INTRODUCTION

The study of relativistic dissipative fluid dynamics has gained significant attention due to its relevance in describing extreme physical conditions such as those in the neutron stars, and ultra relativistic heavy-ion collisions. Among the most established frameworks for relativistic dissipation the oldest and widely used is the Mueller-Israel-Stewart (MIS) theory [1, 2], which addresses the acausality and instability issues inherent in the straightforward relativistic generalization of the Navier-Stokes equations [3, 4]. Among some of the recent improved formulation are DNMR theory [5], developed by Denicol, Niemi, Molnar, and Rischke; BRSSS theory developed by Baier, Romatschke, Son, Starinets, and Stephanov [6], and the BDNK framework, introduced by Bemfica, Disconzi, Noronha, and Kovtun [7].

DNMR is a second-order relativistic hydrodynamics formulation derived from kinetic theory using the 14-moment approximation. It extends the Mueller-Israel-Stewart (MIS) framework by truncating the moment equations to include only the slowest eigenmodes of the linearized collision integral, reducing the number of dynamical variables while maintaining causality and stability [5]. BRSSS is also a second-order relativistic hydrodynamics formulation that ensures causality and conformal invariance, particularly in strongly coupled systems like the quark-gluon plasma (QGP). Meanwhile, BDNK is a first-order approach that still offers causality and stability [8, 9].

MIS theory, rooted in extended irreversible thermodynamics [10], introduces relaxation times for dissipative currents, ensuring a causal and stable evolution under specific conditions [6] and is one of the most widely used formulation of dissipative hydrodynamics in heavy-ion collisions.

The importance of causality in relativistic hydrodynamics originates from the requirement that signal propagation must not exceed the speed of light. This condition is mathematically reflected in the hyperbolicity of the equations of motion, which is guaranteed when the eigenvalues of the characteristic determinant are real, positive and distinct [11]. Although many previous studies [12–28] have analyzed causality and stability mostly in the linear regime, including the effects of shear stress and net charge diffusion, there remains significant scope to explore the hyperbolicity of MIS theory in the context of heat conducting fluids, particularly in the non-linear regime.

This issue is particularly relevant for systems exhibiting significant heat flux [29]. As noted by Hiscock and Lindblom [30], the strict hyperbolicity of the equations of motion can break down when the heat flux becomes extremely large, with the ratio  $|q|/\varepsilon$  reaching some critical values. For instance, they reported that for  $|q|/\varepsilon \approx 0.08898$  for a conformal fluid, the fluid equations cease to be hyperbolic, corresponding to a regime of extraordinarily large heat flux unlikely to be encountered in realistic physical systems. Additionally, they showed that varying transport coeffcients, such as adopting a ten times larger relaxation time through parameter  $\beta_1$ , can extend the hyperbolicity domain to  $|q|/\varepsilon \approx 1/3$ .

In ultrarelativistic heavy-ion collisions, where deviations from equilibrium can be substantial, it is important to explore whether the heat flux values and causality limits predicted by the MIS framework fall within physically realistic ranges. One of the aims of this work is to estimate the typical order of magnitude of heat flux in such systems and investigate the extent of the causality-constrained parameter space. We show that with the current estimate of coefficient of thermal conductivity the heat flow could reach extremely large values for central

fireball temperatures as low as 150 MeV. It is well known that the choice of hydrodynamic frame for defining the fluid four-velocity in dissipative fluids can lead to specific cases such as the Landau frame, where heat flow does not contribute to the energy flux  $T^{0i}$  but reappears as a finite baryon current that is proportional to the thermal conductivity and the gradient of the ratio of chemical potential to temperature [31]. Conversely, one can choose a different frame, such as the Eckart frame, where the dissipative part of the baryon four-current vanishes and the energy flux becomes non-vanishing [32–34].

In this work, we investigate the hyperbolicity of the MIS second-order theory for a heat-conducting fluid in Eckart frame. Our analysis focuses on the dependence of the causality space on the equation of state (EoS), which relates the thermodynamic variables of the fluid. Specifically, we examine the characteristic propagation speed for a one dimensional fluid flow as a function of the ratio of heat flux to fluid energy density,  $q/\varepsilon$ , to determine the parameter space where the theory remains causal. This exploration is crucial for understanding the applicability of the MIS framework to realistic physical scenarios involving significant heat fluxes.

For the equation of state, we adopt both a constant-speed-of-sound EoS,  $p=c_s^2\varepsilon$ , and a realistic lattice QCD EoS, which provides a more accurate representation of strongly interacting matter at high temperatures. By comparing these two cases, we aim to elucidate the EoS dependence of the causality constraints. To keep things simple we disregard here the net baryon density dependence of the speed of sound.

Our study mostly builds upon the formalism presented in [30], where the Eckart frame was used to analyze the stability and hyperbolicity of relativistic heat-conducting fluids. The results of this investigation provide insights into the conditions under which the MIS theory remains hyperbolic (an essential condition for well-posedness) and applicable to systems far from equilibrium, particularly for the early phase of hot and dense nuclear matter produced in high-energy heavy-ion collisions.

The remainder of this paper is organized as follows. In Sec. II, we outline the theoretical framework and governing equations. Sec. III presents the results of our analysis of hyperbolicity and causality for various equations of state and relaxation times. We also discuss the implications of our findings for different equations of state, including a recent lattice QCD equation of state. Furthermore, we include a brief discussion of the second-order coefficient  $\beta_1$ , which is an important parameter controlling the allowed values of  $q/\varepsilon$  for causal wave propagation. Additionally, we provide estimates of heat flow magnitudes using the Navier-Stokes approximation to assess the physical relevance of causality constraints in heavyion collision scenarios. Finally, we summarize our conclusions in Sec. IV.

We use natural units with  $\hbar=c=k_B=1$  throughout the paper. The metric tensor is  $g_{\mu\nu}={\rm diag}(1,-1,-1,-1)$ .

## II. FORMULATION

For simplicity we consider a one-dimensional fluid flow with planar symmetry; the four-velocity of the fluid given by

$$u^{\mu} = (\cosh \rho, \sinh \rho, 0, 0), \tag{1}$$

and the four-vector heat flow  $q^{\mu}=q(\sinh\rho,\cosh\rho,0,0)$ , where the fluid rapidity  $\rho$  is a function of space (x) and time (t). Corresponding fluid acceleration and the expansion scalars are  $a^{\mu}=u^{\nu}\partial_{\nu}u^{\mu}=\left(\cosh\rho\sinh\rho\frac{\partial\rho}{\partial t}+\sinh^2\rho\frac{\partial\rho}{\partial x},\cosh^2\rho\frac{\partial\rho}{\partial t}+\cosh\rho\sinh\rho\frac{\partial\rho}{\partial x},0,0\right)$  and  $\theta=\partial_{\nu}u^{\nu}=\sinh\rho\frac{\partial\rho}{\partial t}+\cosh\rho\frac{\partial\rho}{\partial t}$ . The co-moving derivative in this case is

$$D \equiv u^{\mu} \partial_{\mu} = \cosh \rho \frac{\partial}{\partial t} + \sinh \rho \frac{\partial}{\partial r}.$$

The projection tensor  $\Delta^{\mu\nu} \equiv g^{\mu\nu} - u^{\mu}u^{\nu}$  is

$$\Delta^{\mu\nu} = \begin{bmatrix} -\sinh^2\rho & -\cosh\rho\sin\rho & 0 & 0\\ -\cosh\rho\sinh\rho & -\cosh^2\rho & 0 & 0\\ 0 & 0 & -1 & 0\\ 0 & 0 & 0 & -1 \end{bmatrix}. (2)$$

The energy-momentum tensor  $T^{\mu\nu}$  and the conserved current  $N^{\mu}$  for a dissipative fluid are given by

$$T^{\mu\nu} = \varepsilon u^{\mu} u^{\nu} - (p+\Pi) \Delta^{\mu\nu} + \pi^{\mu\nu} + w^{\mu} u^{\nu} + w^{\nu} u^{\mu} (3)$$
  

$$N^{\mu} = n u^{\mu} + V^{\mu}.$$
 (4)

Where  $\varepsilon$  is the energy density, p is the thermodynamic pressure, related to  $\varepsilon$  via an equation of state (EoS), and  $\Pi$  is the bulk viscous pressure, representing the isotropic deviation of the pressure from its equilibrium value. The shear stress tensor  $\pi^{\mu\nu}$  accounts for anisotropic deviations of the stress tensor and satisfies  $\pi^{\mu\nu}u_{\nu}=0$  and  $\pi^{\mu\nu}\Delta_{\mu\nu}=0$ . The energy flux four-vector  $w^{\mu}$  represents the flow of energy relative to the fluid's rest frame and satisfies  $w^{\mu}u_{\mu}=0$ . In the conserved current  $N^{\mu}$ , n is the density of the conserved quantity (e.g., net baryon), while  $V^{\mu}$  is the particle diffusion current, representing deviations of the particle flux from the equilibrium rest frame, and it satisfies  $V^{\mu}u_{\mu}=0$ . The definitions of these quantities in terms of energy momentum tesnsor are as follows:

$$\begin{split} \varepsilon &= u_{\mu}u_{\nu}T^{\mu\nu},\\ \Pi + p &= -\frac{1}{3}\Delta\mu\nu T^{\mu\nu},\\ \pi^{\mu\nu} &= \left[\frac{1}{2}\left(\Delta^{\mu\sigma}\Delta^{\nu\tau} + \Delta^{\nu\sigma}\Delta^{\mu\tau}\right) - \frac{1}{3}\Delta^{\mu\nu}\Delta^{\sigma\tau}\right]T_{\tau\sigma},\\ V^{\mu} &= \Delta^{\mu\nu}N_{\nu},\\ w^{\mu} &= \frac{\varepsilon + p}{n}V^{\mu} + q^{\mu},\\ n &= u_{\mu}N^{\mu}. \end{split}$$

We choose Eckart frame (where particle three current  $V^{\mu}$  vanishes) for defining our hydrodynamic four velocity; by definition the particle diffusion  $V^{\mu}$  is zero in this frame, and the energy flow  $w^{\mu}$  coincides with the heat flow  $q^{\mu}$ . It is important to note that the coefficient of thermal conductivity  $\kappa$  (defined below) may diverge for a QCD medium containing equal number of quark and antiquarks. In the limit where the quark chemical potential  $\mu \ll T$ , this divergence scales as  $\sim 1/\mu^2$ . Despite the divergent  $\kappa$ , the correction to the baryon current remains finite. This makes the Landau-Lifshitz frame a more suitable choice than the Eckart frame for systems produced at vanishingly small baryon chemical potential, as discussed in Ref. [31]. For simplicity, we neglect shear and bulk viscosity in this study. The conservation equations and the Muller-Israel-Stewart (MIS) evolution equation

for heat flow reduce to the following form:

$$Dn + n\theta = 0(5)$$

$$D\varepsilon + (\varepsilon + p)\theta - 2q^{\mu}a_{\mu} + \nabla_{\mu}q^{\mu} = 0(6)$$

$$(\varepsilon + p)Du^{\alpha} - \nabla^{\alpha}p + q^{\mu}\partial_{\mu}u^{\alpha} + \Delta^{\alpha\nu}Dq_{\nu} + q^{\alpha}\theta = 0(7)$$

$$\tau_{q}\Delta^{\mu\nu}\dot{q}_{\nu} + q^{\mu} + \kappa\left(\nabla^{\mu}T - T\dot{u}^{\mu}\right)$$

$$+ \left[\frac{1}{2}\kappa T^{2}\partial_{\nu}\left(\frac{\tau_{q}}{\kappa T^{2}}u^{\nu}\right)q^{\mu}\right] = 0(8)$$

Here, the relaxation time for heat flow is given by  $\tau_q = \kappa T \beta_1$ , where  $\kappa$  is the coefficient of thermal conductivity, and  $\beta_1$  is a second-order transport coefficient. Following Ref. [30], we take  $\beta_1$  to be a multiple  $\lambda$  of its expression in the Israel-Stewart theory for an ultra-relativistic gas, i.e.,  $\beta_1 = \lambda \frac{5}{4p}$ . The parameter  $\lambda = 0$  corresponds to the acausal first-order (Navier-Stokes) theory.

For the one dimensional flow Eq.(1), and EoS  $p=c_s^2\varepsilon=nT$  the conservation equatons Eq.(5) - Eq.(8) take the following form,

$$\cosh \rho \frac{\partial n}{\partial t} + \sinh \rho \frac{\partial n}{\partial x} + n \sinh \rho \frac{\partial \rho}{\partial t} + n \cosh \rho \frac{\partial \rho}{\partial x} = 0.$$
 (9)

$$\cosh \rho \frac{\partial \varepsilon}{\partial t} + \sinh \rho \frac{\partial \varepsilon}{\partial x} + \left[ \varepsilon (1 + c_s^2) \sinh \rho + 2q \cosh \rho \right] \frac{\partial \rho}{\partial t} 
+ \left[ \varepsilon (1 + c_s^2) \cosh \rho + 2q \sinh \rho \right] \frac{\partial \rho}{\partial x} + \sinh \rho \frac{\partial q}{\partial t} + \cosh \rho \frac{\partial q}{\partial x} = 0,$$
(10)

$$c_s^2 \sinh \rho \frac{\partial \varepsilon}{\partial t} + c_s^2 \cosh \rho \frac{\partial \varepsilon}{\partial x} + \cosh \rho \frac{\partial q}{\partial t} + \sinh \rho \frac{\partial q}{\partial x} + \left[ \varepsilon (1 + c_s^2) \cosh \rho + 2q \sinh \rho \right] \frac{\partial \rho}{\partial t} + \left[ \varepsilon (1 + c_s^2) \sinh \rho + 2q \cosh \rho \right] \frac{\partial \rho}{\partial x} = 0, \tag{11}$$

$$\left[\frac{\sinh\rho}{\varepsilon} - \frac{10\lambda q}{8\varepsilon^2 c_s^2}\cosh\rho\right] \frac{\partial\varepsilon}{\partial t} + \left[\frac{\cosh\rho}{\varepsilon} - \frac{10\lambda q}{8\varepsilon^2 c_s^2}\sinh\rho\right] \frac{\partial\varepsilon}{\partial x} 
- \frac{1}{n} \left[\sinh\rho - \frac{5\lambda q}{8\varepsilon c_s^2}\cosh\rho\right] \frac{\partial n}{\partial t} - \frac{1}{n} \left[\cosh\rho - \frac{5\lambda q}{8\varepsilon c_s^2}\sinh\rho\right] \frac{\partial n}{\partial x} + \frac{5\lambda}{4\varepsilon c_s^2}\cosh\rho \frac{\partial q}{\partial t} 
+ \frac{5\lambda}{4\varepsilon c_s^2}\sinh\rho \frac{\partial q}{\partial x} + \left[\cosh\rho + \frac{5\lambda q}{8\varepsilon c_s^2}\sinh\rho\right] \frac{\partial\rho}{\partial t} + \left[\sinh\rho + \frac{5\lambda q}{8\varepsilon c_s^2}\cosh\rho\right] \frac{\partial\rho}{\partial x} + \frac{3qn}{k\varepsilon} = 0.$$
(12)

Here we have eliminated T, and p in terms of  $\varepsilon$  and n. Equations (9) - (12) are a set of closed equations of the four variables  $Y^{\nu} = (n, \varepsilon, \rho, q)$ . These set of equations are known to be hyperbolic (causal speed of wave propagation) if the eigenvalues are real and distinct. To calculate the characteristic speed (eigenvalues) it is usual practice to write the above set of equations in the following form

$$A^{\mu a}_{\nu}\partial_{\alpha}Y^{\nu} + B^{\mu} = 0. \tag{13}$$

where  $\nu \to \text{fluid variables } (n, \varepsilon, \rho, q), \ \mu \to \text{equations } (9)$  - (12),  $a \to \text{corresponds to } (t, x, y, z), \text{ since we have a}$ 

planar symmetry there is no y, z dependence. The characteristic velocities are obtained from the determinant of the following characteristic matrix

$$M = vA^{\mu t}_{\nu} - A^{\mu x}_{\nu}. \tag{14}$$

We will rewrite each equation to identify the coefficients  $A^{\mu a}_{\nu}$  and  $B^{\mu}$ . The explicit forms of the matrix elements  $A^{\mu a}_{\nu}$  and  $B^{\mu}$  are described in detail in appendix A. Without loss of generality, we can construct the matrix M in the fluids rest frame  $\rho = 0$ , in this case the analysis be-

come simpler and we have

$$M = \begin{pmatrix} v & 0 & -n & 0\\ 0 & v & 2qv - (1+c_s^2)\varepsilon & -1\\ 0 & -c_s^2 & (1+c_s^2)\varepsilon v - 2q & v\\ \frac{5\lambda qv}{8\varepsilon c_s^2 n} + \frac{1}{n} & -\frac{10\lambda qv}{8\varepsilon^2 c_s^2} - \frac{1}{\varepsilon} & v - \frac{5\lambda q}{8\varepsilon c_s^2} & \frac{5\lambda v}{4\varepsilon c_s^2} \end{pmatrix}$$

$$\tag{15}$$

Setting det(M) = 0 we get the equation for characteristic velocities

$$\left[\frac{5\lambda}{4}\left(1+\frac{1}{c_s^2}\right) - \frac{5\lambda q^2}{2c_s^2\varepsilon^2} - 1\right]v^4 + \left[\frac{5\lambda q}{2\varepsilon}\left(1-\frac{1}{c_s^2}\right) - \frac{2q}{\varepsilon}\right]v^3 + \left[c_s^2 - 1 - \frac{5\lambda}{4}(1+c_s^2) + \frac{5\lambda q^2}{2c_s^2\varepsilon^2}\right]v^2 + 2\frac{q}{\varepsilon}v + c_s^2 = 0. \tag{16}$$

The characteristic velocities are obtained by solving Eq.(16) numerically; for a given value of  $\lambda$ ,  $c_s^2$  we study whether four real roots exist.

#### III. RESULT

We begin by fixing  $\lambda=1$ , which corresponds to  $\beta_1=\frac{5}{4p}$ , i.e., the second-order transport coefficient is set to its ultra-relativistic limit according to kinetic theory. The numerical roots for the characteristic velocities v are computed for four different values of the squared speed of sound,  $c_s^2=0.05,0.1,0.33,0.5$ . These results are displayed in four panels of Fig. 1. Although a relativistic massless gas has  $c_s^2=1/3$ , one of the values choosen here  $c_s^2=0.5$  is higher than this limit, we choose this value based on the fact that for extremely dense systems  $c_s^2$  known to exceed the relativistic massless gas limit and may approach  $c_s^2\to 1$  (see e.g. Kapusta and Gale [35], Weinberg[36], Bedaque and Steiner 2015 [37]).

From the top and bottom panels of Fig. 1, we observe that for all four scenarios, a causal region with four distinct real roots exists for  $|\frac{q}{\varepsilon}|$  within a range  $\approx 0.2$  around the origin. In particular, the causal region expands to higher values of  $|\frac{q}{\varepsilon}|$  as  $c_s^2$  increases. This behavior clearly shows the dependence of causality on the equation of state through  $c_s^2$ .

The result for a massless ultra-relativistic gas  $(c_s^2 = \frac{1}{3})$  is shown in the bottom-left plot of Fig. 1. We observe that for  $|q/\varepsilon| < 0.18$ , the characteristic speeds lie approximately in the range 0.45 < v < 0.63. This finding is consistent with the results reported by Hiscock and Lindblom [30].

To further investigate the dependence of causality on the relaxation parameter  $\lambda$ , we consider two arbitrarily chosen values: a smaller  $\lambda=0.75$  and a larger  $\lambda=10$ . We first examine the case  $\lambda=0.75$ , with the corresponding characteristic velocities shown in Fig. 2. Similar to the  $\lambda=1$  case, we find that the causal region expands with increasing  $c_s^2$ . However, the range of  $|\frac{q}{\varepsilon}|$  over which causality is preserved is somewhat narrower than in the

 $\lambda=1$  scenario, with a pronounced reduction in the causal region at smaller values of  $c_s^2$ . As we will see later, Lattice QCD calculations indicate that  $c_s^2$  in the temperature range relevant for heavy-ion collisions reaches values around  $\sim 0.15$  near the crossover temperature (see Fig. 4). This observation shows that the relaxation time, encoded in the parameter  $\lambda$ , also plays an important role in determining the system's causality.

We now consider the case where  $\lambda=10.$  This value represents a significantly larger relaxation time compared to the previously analyzed cases ( $\lambda=1$  and  $\lambda=0.75).$  The characteristic velocities v as functions of  $\frac{q}{\varepsilon}$  for four different values of  $c_s^2=0.05,0.1,0.33$ , and 0.5 are shown in Fig. 3.

From Fig. 3, we observe that the causal region becomes less constrained as  $\lambda$  increases. Like other  $\lambda$  values here also we observe for small values of  $c_s^2$  (e.g.,  $c_s^2=0.05$  and  $c_s^2=0.1$ ), the range of  $|\frac{q}{\varepsilon}|$  for which all four roots remain real and distinct is significantly reduced compared to the cases of larger  $c_s^2$ . This indicates that although a larger relaxation time tends to instate causality in the system, the equation of state imposes constraint making it nontrivial to apply second-order hydrodynamics for systems with large gradients.

For larger values of  $c_s^2$ , such as  $c_s^2=0.33$  (the ultrarelativistic limit) and  $c_s^2=0.5$ , the causal region remains relatively robust, and allows a very large range of  $\frac{q}{\varepsilon}$  compared to smaller cases  $\lambda$ . Since MIS theory consider the dissipative corrections are to be smaller, it is not known exactly how large the heat flow could be considered before the theory breaks down. Notably, for  $c_s^2=0.33$ , the characteristic velocities lie within the sub-luminal range (v<1) only for  $|q/\varepsilon|<0.25$ . This suggests that in the ultra-relativistic regime, larger relaxation time ensure causality in systems with a large gradient of temperature.

Our findings shows the critical role of the relaxation parameter  $\lambda$  as well as EoS in determining the causality (and hence the stability) of relativistic fluid with non-zero heat flow. While moderate values of  $\lambda$  (e.g.,  $\lambda=1$ ) allow for broader causal regions, smaller values of  $\lambda$  severely restrict the range of  $\frac{g}{\varepsilon}$  for which causality is preserved.

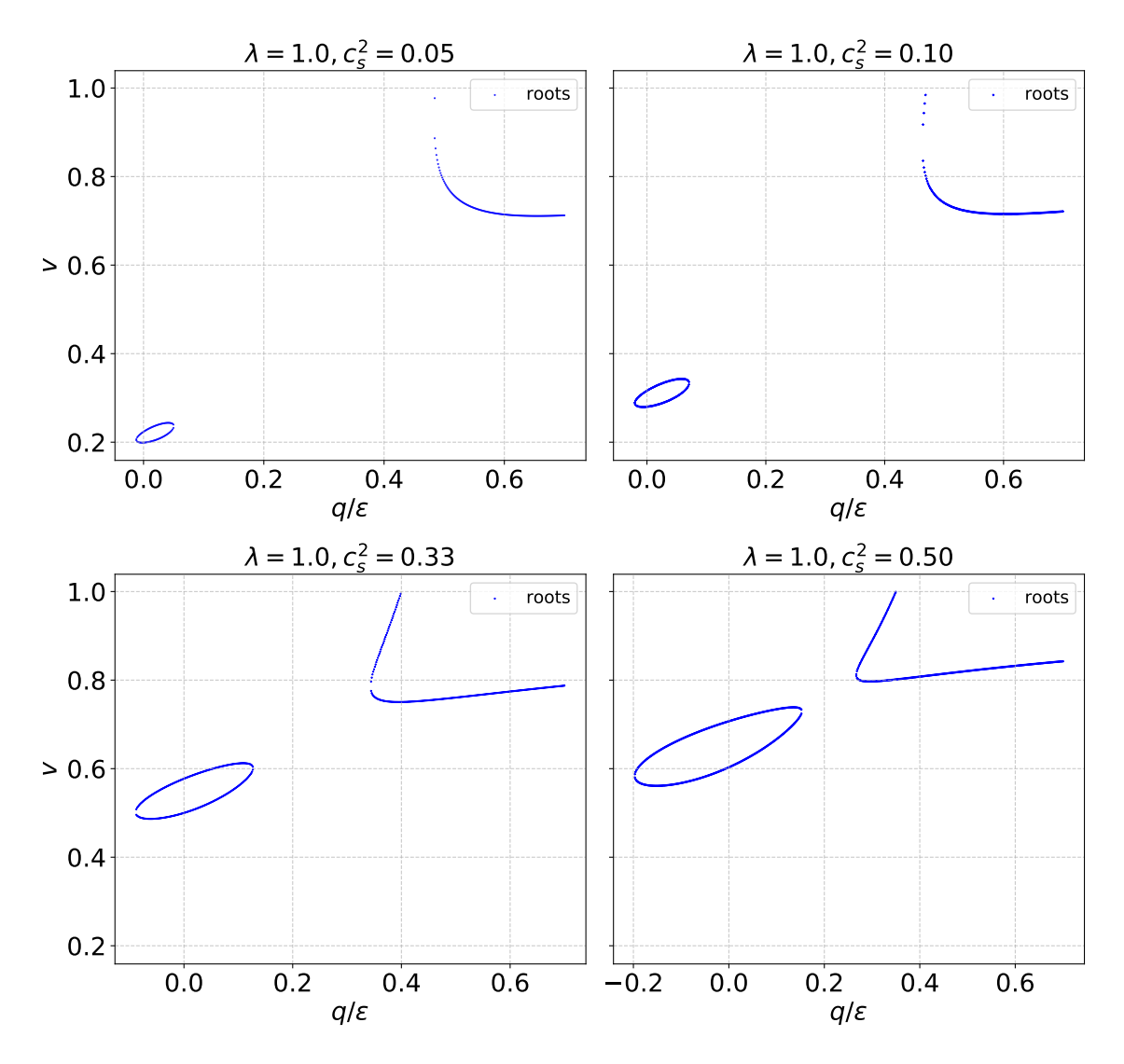


FIG. 1. Characteristic velocities v obtained from the numerical solution of Eq. (16) shown as a function of  $q/\varepsilon$ , for  $\beta_1 = \frac{5}{4p}$  and four different  $c_s^2 = 0.05$ , 0.10, 0.33, and 0.5.

This behavior is demanding the importance of carefully calibrating  $\lambda$  based on the physical properties of the system under study.

The results presented above demonstrate the important interplay between the equation of state through  $c_s^2$ , the relaxation parameter  $\lambda$ , and the relative magnitude of the heat flow  $\frac{q}{\varepsilon}$  in determining the causal structure of relativistic fluids. Our findings confirm that causality is preserved only within specific ranges of  $\frac{q}{\varepsilon}$ , which depend sensitively on both  $c_s^2$  and  $\lambda$ .

For  $c_s^2 = \frac{1}{3}$ , which corresponds to the ultra-relativistic limit, the characteristic velocities remain subluminal (v < 1) for small values of  $|q/\varepsilon|$ . The expansion of the causal region with increasing  $c_s^2$  suggests that stiffer equations of state are more conducive to maintaining causality.

## A. $c_s^2(\varepsilon)$ from Lattice QCD result

Up until now, we have shown the results for a temperature-independent constant speed of sound. But in reality, the speed of sound depends on both temperature and density. Here, we consider only the temperature dependence of  $c_s^2$ ; the inclusion of density dependence could be done in a similar fashion.

To study the realistic scenario of a temperature-dependent  $c_s^2$ , we use LQCD results from Ref. [38]. We use the tabulated data for thermodynamic variables provided in [38] for the  $N_f=2+1$  QCD equation of state as a function of temperature and convert it to express  $c_s^2$  as a function of  $\varepsilon$  for use in our calculation. The corresponding plot for  $c_s^2$  as a function of  $\varepsilon$  is shown in Fig. (4). As can be seen from Fig. (4),  $c_s^2$  exhibits a non-monotonic variation, with a dip around  $\sim 130~{\rm MeV}$  and approaching the massless limit  $c_s^2=\frac{1}{3}$  from below in

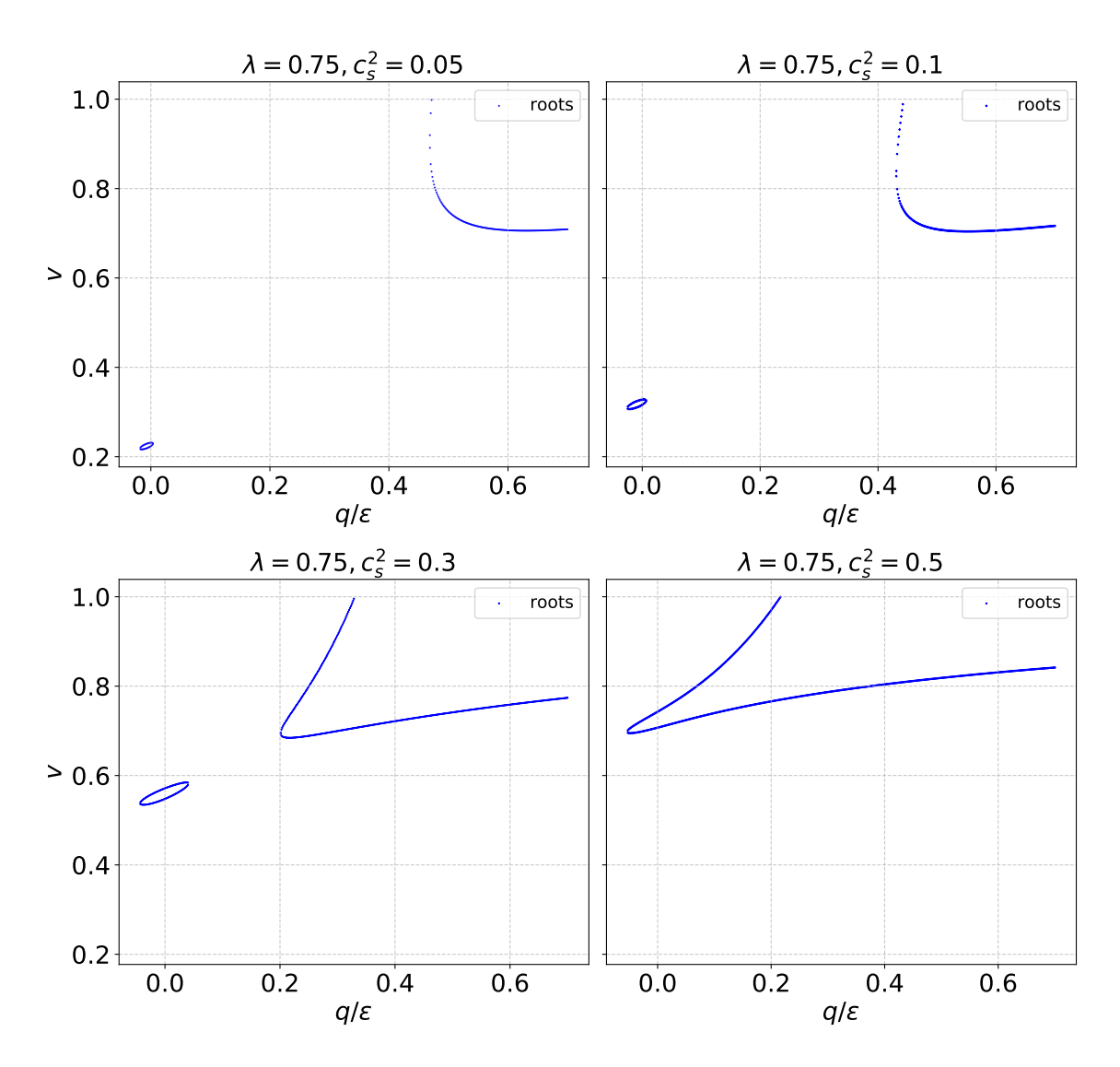


FIG. 2. Same as Fig.(1) but for  $\lambda = 0.75$ .

the high-temperature regime. This non-trivial temperature dependence of the speed of sound has interesting implications for the corresponding causal region.

The characteristic velocities v for three different values of the relaxation parameter  $\lambda=0.5,1.0,$  and 20.0 are shown in Fig. 5 for the temperature-dependent speed of sound as shown in Fig. 4.

From the top panel of Fig. 5 corresponding to  $\lambda=0.5$ , we observe that the characteristic velocities exhibit significant variation over a relatively wide range of  $q/\varepsilon$ , with regions of multiple real roots indicating causal propagation. However, the structure is considerably more intricate compared to the constant  $c_s^2$  case, with more pronounced non-linearities in the velocity profile. The causal region appears to extend into both positive and negative values of  $q/\varepsilon$ , though the subluminal condition v<1 may be violated in some regions, indicating instability for extreme gradients.

The middle panel shows the result for  $\lambda = 1.0$ . Here,

the causal region is more tightly constrained, and the structure of the velocity curves is comparatively simpler than for  $\lambda=0.5$ . We find that for small values of  $q/\varepsilon$ , all four roots remain real and subluminal, while beyond a certain threshold the number of real roots reduces, signaling a loss of causality. Compared to the constant  $c_s^2$  scenario, the causal region is somewhat suppressed, likely due to the dip in  $c_s^2$  around the crossover region in the LQCD equation of state.

The bottom panel corresponds to a much larger relaxation parameter,  $\lambda=20.0$ , representing a system with significantly delayed relaxation to equilibrium. In this case, we again observe a complex structure of the characteristic velocities, but the causal region appears to broaden compared to the  $\lambda=1.0$  case, consistent with the trend that increasing  $\lambda$  tends to support causality over a wider range of heat flux. However, similar to the  $\lambda=0.5$  case, the high degree of non-linearity in the velocity structure can introduce regions where some roots

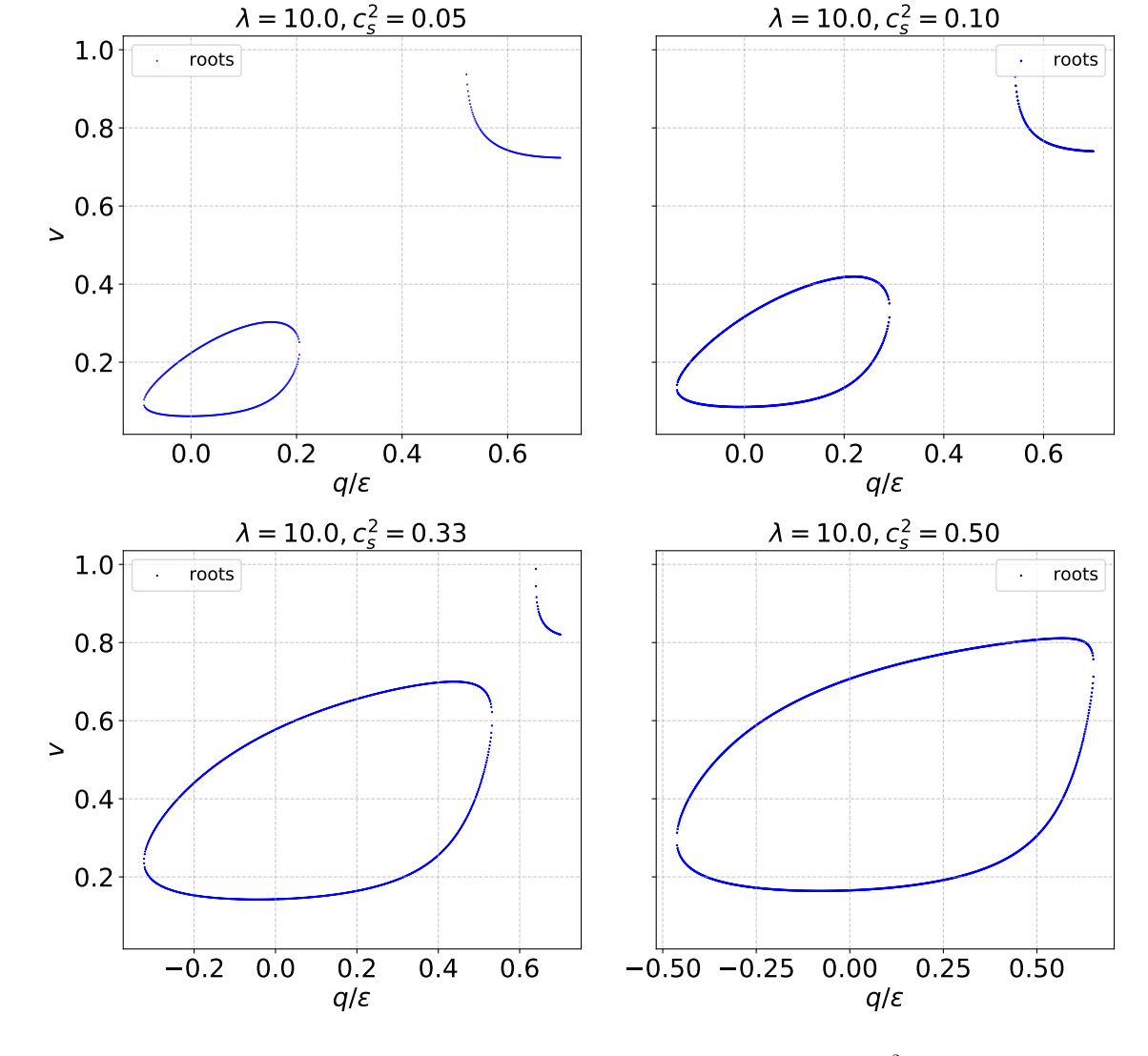


FIG. 3. Characteristic velocities v as functions of  $\frac{q}{\varepsilon}$  for  $\lambda=10$  and four different values of  $c_s^2$ : 0.05, 0.1, 0.33, 0.5. The causal regions are showing a significant enhancement in the range of  $\frac{q}{\varepsilon}$  compared to smaller  $\lambda$  cases.

may exceed the light cone or become complex.

Overall, the figure highlights that the use of a realistic, temperature-dependent speed of sound introduces substantial modifications to the causal structure compared to the idealized constant  $c_s^2$  case. In particular, the dip in  $c_s^2$  near  $T\sim 130$  MeV seen in LQCD results leads to a narrowing of the causal window for intermediate energy densities.

## 1. Discussion on $\beta_1$

As it is clear from the above discussion that the causal parameter space is quite sensitive to the second-order transport coefficient  $\beta_1$  appearing in MIS theory for heat flow. It is worthwhile to discuss its physical values for the temperature ranges we are interested in. Kinetic theory calculation based on Grad's fourteen moment method for

a Boltzmann gas gives the following values for  $\beta_1 P$  for ultra-relativisitic ( $z \ll 1$ ), non-relativistic ( $z \gg 1$ ) and in the intermediate ( $z \sim 1$ ) regions

$$\beta_1 P = \begin{cases} \frac{5}{4}, & \text{for } z \ll 1 \text{ (Ultra-relativistic)} \\ \frac{2}{5}z, & \text{for } z \gg 1 \text{ (Non-relativistic)} \\ \left(\frac{\gamma - 1}{\gamma}\right)^2 \cdot \frac{z}{y} \cdot \left(5y^2 - X\right), & \text{otherwise} \end{cases}$$

where

$$y = \frac{K_3(z)}{K_2(z)},\tag{17}$$

$$X = z^2 \left( 1 + \frac{5y}{z} - y^2 \right), \tag{18}$$

$$\gamma = \frac{X}{X - 1},\tag{19}$$

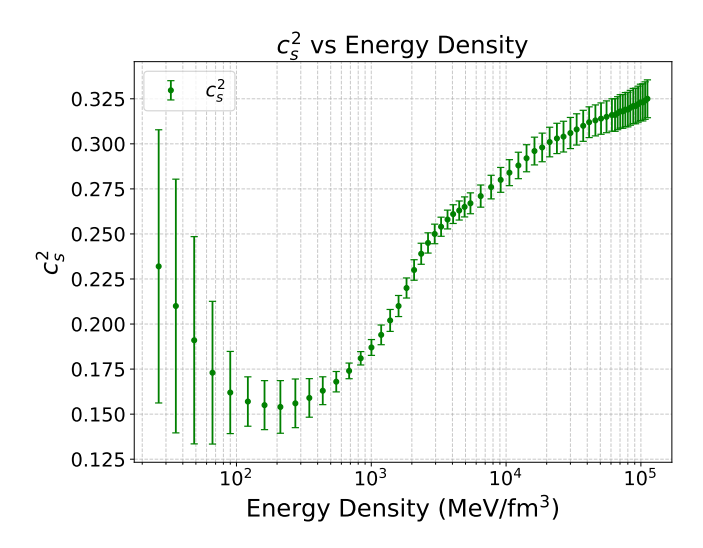


FIG. 4. Lattice QCD results for squared speed of sound  $c_s^2$  as a function of energy density.

 $z = \frac{m}{T}$ , and  $K_n(z)$  denotes the modified Bessel function of the second kind of order n.

Fig.(6) shows the variation of  $\beta_1 P$  as a function of z. As can be seen lower temperature (larger z) corresponds to larger  $\beta_1$  which implies larger relaxation time for heat flow. On the other hand the large temperature limit gives  $\beta_1 \propto \frac{1}{p}$  that implies  $\beta_1$  becomes smaller as we approach high-temperature limit.

## 2. Estimation of heat flow in the Navier-Stokes limit

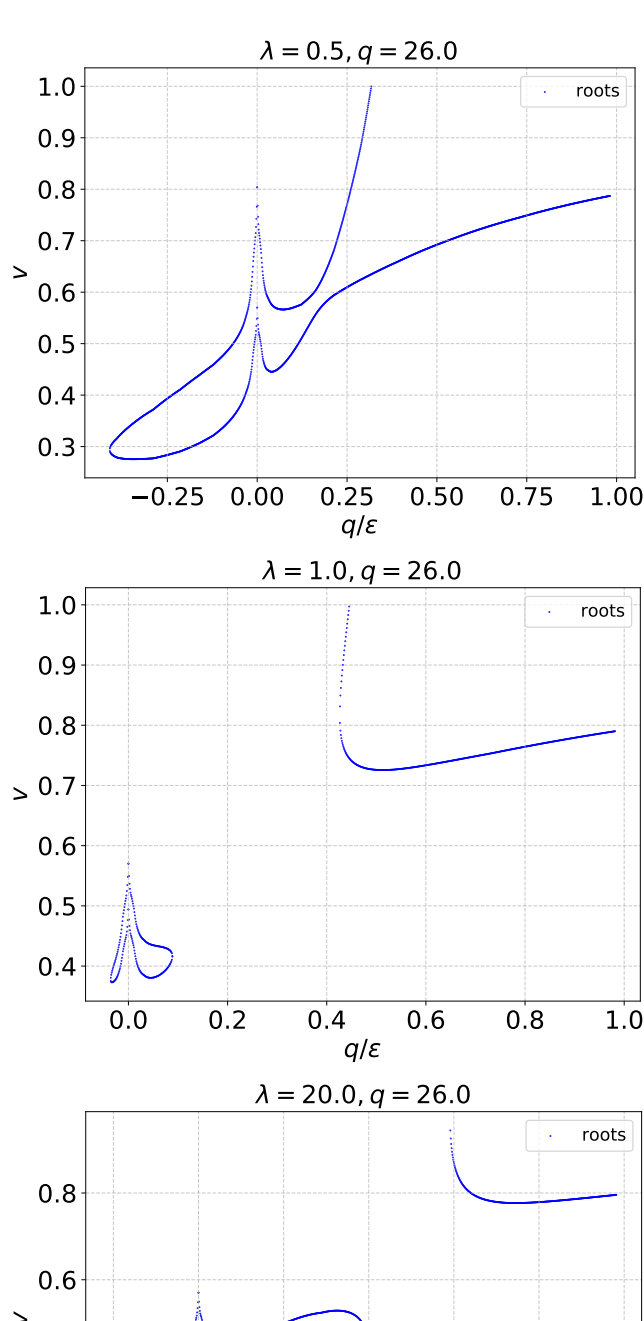
At this point, it is interesting to obtain an order-of-magnitude estimate of the heat flow values that occur in RHIC and lower-energy collisions to assess the causal zones allowed by the MIS theory. Let us consider the simplest Navier-Stokes approximation of the heat flow equation ( $\tau_q \to 0$ ) that implies the heat flux responds almost instantaneously to changes in the thermodynamic gradients, thereby eliminating the "memory" effects that are characteristic of the Israel-Stewart formulation. Eq. (8) in this limit takes the following form:

$$q^{\mu} + \kappa \left( \nabla^{\mu} T - T \dot{u}^{\mu} \right) = 0. \tag{20}$$

The above equation states that the heat flux is directly proportional to the spatial gradient of temperature and an additional relativistic term involving the fluid's acceleration. For further simplification, let us use the zeroth-order equation of motion and set  $\dot{u}^{\mu} = \frac{\nabla^{\mu} p}{(\varepsilon + p)}$  in Eq. (20). This gives us the Navier-Stokes expression for heat flow as

$$q^{\mu} = -\kappa \left( \nabla^{\mu} T - \frac{T}{(\varepsilon + p)} \nabla^{\mu} p \right). \tag{21}$$

If we disregard the fluid acceleration by setting  $\dot{u}^{\mu} = 0$  in Eq. (20), we obtain the simplest approximation  $q^{\mu} =$ 



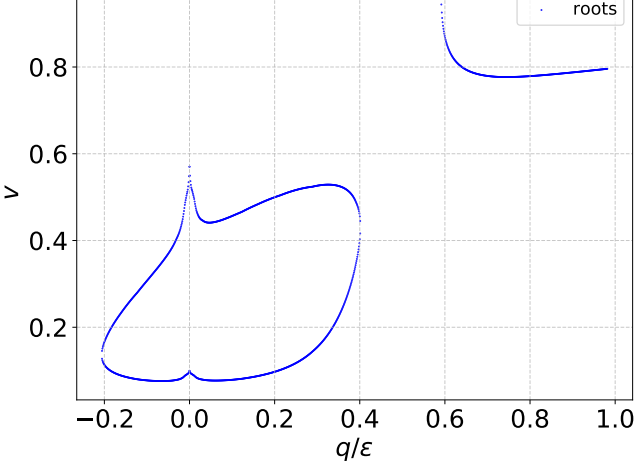


FIG. 5. Characteristic velocities v as functions of  $\frac{q}{\varepsilon}$  for three different  $\lambda=0.5,\,1.0,\,$  and 20 and for speed of sound obtained from lattice QCD equation of state. The causal regions are showing a significant changes compared to the temperature independent constant speed of sound case.

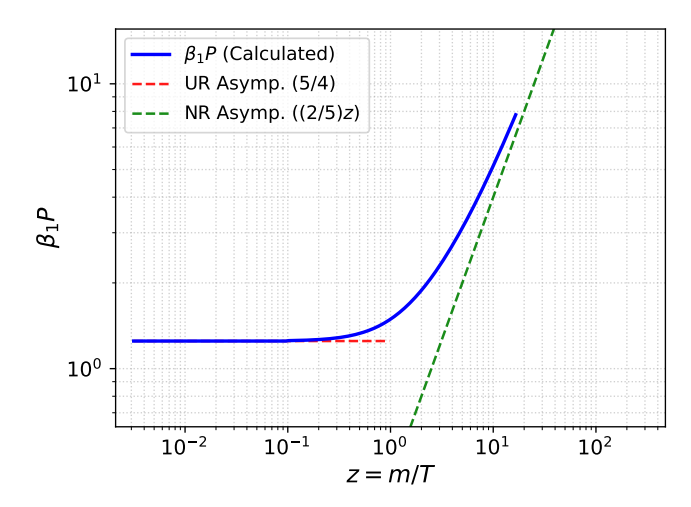


FIG. 6. Second order coefficient  $\beta_1$  times pressure as a function of  $z = \frac{m}{T}$ . The red and green dashed lines are ultrarelativistic and non-relativistic limits respectively, and the solid blue line is the exact calculation.

 $-\kappa \nabla^{\mu} T$ . Below, we will show the individual and combined contributions to the total heat flux from the temperature gradient and pressure gradient. We are primarily interested in the ratio of the magnitude of the spatial part of the heat flow vector to energy density, i.e.,  $|\mathbf{q}|/\varepsilon$ . To obtain  $|\mathbf{q}|$ , we need to provide appropriate values for  $\kappa$ . To the best of our knowledge, first-principle lattice QCD results for thermal conductivity  $\kappa$  are not currently available, mainly due to theoretical constraints and technical challenges involved in extracting the necessary correlation functions, especially since thermal conductivity is only an independent transport coefficient in the presence of conserved charges. However, several QCDinspired model calculations (notably BGK/quasiparticle models) do provide estimates and qualitative insights into the behavior of thermal conductivity in hot and dense QCD matter. For example,  $\kappa$  has been calculated from relativistic kinetic theory and the NJL model in [31, 39– 43], etc.

However, all these studies provided varying temperature dependence of  $\kappa$ . For example, in [31], the expression for  $\kappa$  in the small  $\mu/T$  and symmetric quark-antiquark  $|n_q-n_{\bar{q}}| \ll (n_q+n_{\bar{q}})$  limit is

$$\kappa = \frac{16}{9} \frac{K_{\rm SB}^2}{N_c N_f} (\tau_q T) \frac{T^4}{\mu^2}, \tag{22}$$

where  $K_{\rm SB} = \left[\left(N_c^2-1\right) + 7N_cN_f/8\right]\pi^2/15$  is the Stefan-Boltzmann constant for  $N_f$  flavors and  $N_c$  colors, and  $\tau_q T$  was shown to be proportional to  $1/(\alpha_s^2 \ln(1/\alpha_s))$ . According to the above formulation,  $\kappa/T^2$  should increase as a function of temperature for a given  $\mu/T$ , since the strong coupling  $\alpha_s$  decreases as a function of temperature. For simplicity, we performed our calculation for a system with a characteristic radius of R=5 fm and central temperature of  $T_0=200$  MeV. We further assume the temperature varies linearly along the

radial direction:  $T(r) = T_0 \left(1 - \frac{r}{R}\right)$ . Using Eq. (22), we calculate  $\kappa$  for different  $\mu/T$  values as given in Table I, where we used  $N_c = 3$  and  $N_f = 2$  with the one-loop result for running  $\alpha_s$  in the calculation. The heat flow for such a linear radial dependence of temperature and for  $\mu/T = 0.1$  and central temperature  $T_0 = 200$  MeV is  $|\mathbf{q}_{\nabla T}| \approx 711$  GeV/fm<sup>3</sup>. Where we consider only the simplest approximation driven by the temperature gradient  $(q^i \approx -\kappa \nabla^i T)$ . The thermal conductivity is taken to be  $\kappa = 6.9 \times 10^8$  MeV<sup>2</sup>. For the thermodynamic quantities, we use the Wuppertal-Budapest lattice QCD equation of state [38].

Next, we include the correction term from Eq. (21). This term, which accounts for the pressure gradient, provides a contribution that opposes the primary heat flow. For the given parameters, its magnitude is calculated to be  $|\mathbf{q}_{\nabla p}| \approx 108~\text{GeV/fm}^3$ . The inclusion of this correction term results in a total heat flux of  $|\mathbf{q}_{\text{total}}| \approx 603~\text{GeV/fm}^3$ . This shows that the pressure gradient provides a significant, non-trivial contribution, reducing the magnitude of the heat flow by approximately 15% compared to the simple gradient approximation. The resulting ratio of the total heat flux to the central energy density is found to be  $|\mathbf{q}_{\text{total}}|/\varepsilon_0 \approx 330$ , where we take  $\varepsilon_0 \sim 1.8~\text{GeV/fm}^3$  at T=200~MeV temperature. It is evident that  $|\mathbf{q}_{\text{total}}|/\varepsilon_0 \approx 330~\text{is}$  too large a value to be physically realistic.

$\mu/T$	$\kappa \; (\mathrm{MeV^2})$
0.10	$6.92 \times 10^{8}$
0.30	$7.69 \times 10^{7}$
0.50	$2.77 \times 10^7$

TABLE I. Heat conductivity  $\kappa$  as a function of  $\mu/T$  for  $N_c=3,\ N_f=2$  at a fixed temperature of T=200 MeV.

Similar calculations for a somewhat lower central temperature T=150 MeV and  $\mu/T=0.1$ , but keeping other parameters fixed, result in a somewhat larger  $|\mathbf{q}_{\rm total}|/\varepsilon_0\approx 811$  (where  $\kappa\approx 3.31\times 10^8$  MeV<sup>2</sup> is taken from Table II). The apparent increase in  $|\mathbf{q}_{\rm total}|/\varepsilon_0$  for lower temperature is due to the fact that  $\varepsilon\sim T^4$ , whereas  $\kappa\sim T^2$ .

Larger values of  $\mu/T$  will not lead to a significant decrease in the heat flow because  $\kappa$  changes by only one order of magnitude as we increase  $\mu/T$  from 0.1 to 0.5. Hence, this will not give us any acceptable values for  $|\mathbf{q}|/\varepsilon$  either. On the other hand, if  $\kappa$  is hypothetically taken to be two orders of magnitude smaller, i.e.,  $\kappa \sim 10^5 \text{ MeV}^2$ , that will give us  $|\mathbf{q}_{\text{total}}|/\varepsilon \sim 0.24$  at T=150 MeV, which is somewhat reasonable but still considered to be a large value.

Since it is clear that the large heat flow originates mainly due to the large value of  $\kappa$ , it is worthwhile to check its value from other theoretical model studies. A more recent calculation [40] based on semi-classical transport theory using a quasi-particle description of a system of quarks, antiquarks, and gluons with a realistic QCD

equation of state gives a somewhat different temperature dependence (for non-zero quark chemical potentials):

$$\kappa = \begin{cases} \sim 150 \times T^2, & \text{for } T/T_c \sim 1.5, \\ \\ \sim 25 \times T^2, & \text{for } T/T_c \sim 5. \end{cases}$$

If we consider  $T_c \sim 150$  MeV, this corresponds to  $\kappa \sim 7.5 \times 10^6$  MeV<sup>2</sup> at T=225 MeV and  $\kappa \sim 1.4 \times 10^7$  MeV<sup>2</sup> at T=750 MeV. These values are comparable to what we reported in Tables I and II. The thermal conductivity coefficient was calculated in [42] using a numerical solution of the relativistic Boltzmann equation for a classical gas of massless particles with elastic binary collisions and constant isotropic cross-section, and in Ref. [43] using the NJL model. These results are in good agreement with the above reported values.

$\overline{\mu/T}$	$\kappa \; (\mathrm{MeV}^2)$
0.10	$3.31 \times 10^{8}$
0.30	$3.68 \times 10^{7}$
0.50	$1.32 \times 10^7$

TABLE II. Heat conductivity  $\kappa$  as a function of  $\mu/T$  for  $N_c=3, N_f=2$  at a fixed temperature of T=150 MeV.

At this point, we would like to mention that the decisive factor for large heat flow is the value of  $\kappa$  used here, which is obtained from kinetic theory calculations; a first-principle calculation of  $\kappa$  from lattice QCD is required to obtain an accurate estimate of the heat flow. We should also note that the above calculation is performed in the Navier-Stokes limit, and as we know from the MIS theory, heat flow is a dynamical variable like other dissipative quantities and will follow a transient behavior where its magnitude during the initial times could be very different (and large) from the Navier-Stokes limit and only approaches it at late times. This implies that causality criteria in heavy-ion collisions related to heat flow are on the brink or perhaps broken, a fact which is also shown in numerical studies [45] but for non-zero shear and bulk viscosities. This question is more relevant for smaller systems, such as proton-proton collisions or peripheral heavy-ion collisions, with larger temperature gradients.

## IV. CONCLUSION

In conclusion, we have analyzed the causality conditions for a one-dimensional relativistic fluid with heat flow. By solving the characteristic equation numerically, we determined the ranges of  $\frac{q}{\varepsilon}$  for which the system exhibits hyperbolic behavior, ensuring causal propagation of signals. Our results shows that both the equation of state and the relaxation time significantly influence the causal structure of the system.

To maintain causality, the eigenvalues of the characteristic equations must be real and respect subluminal signal propagation conditions. The constraints on relaxation times for dissipative stresses are crucial in this regard, as improper values may introduce acausal modes or instabilities. The exact constraints require solving for the eigenvalues explicitly and analyzing their dependence on the transport coefficients.

In the Navier-Stokes limit, we further estimated the ratio of heat flow to the fluid central energy density under certain simplified assumptions. The corresponding values turned out to be unrealistically large ( $|\mathbf{q}_{\text{total}}|/\varepsilon_0 \approx 330$  for T=200 MeV and  $\approx 811$  for T=150 MeV) for the temperature range and thermal conductivity  $\kappa$  values obtained from theoretical model studies applicable to RHIC and lower-energy heavy-ion collisions. These results suggest that either the current estimates of thermal conductivity are overestimated, or that the applicability of dissipative fluid dynamics breaks down in these extreme conditions.

Our analysis reveals that the pressure gradient correction provides a non-trivial contribution, reducing the heat flow magnitude by approximately 15% compared to the simple temperature gradient approximation. However, even with this correction, the heat flow remains orders of magnitude larger than what would be considered physically reasonable.

We believe that first-principle calculations of  $\kappa$  from lattice QCD are essential for better constraining the causal parameter space and providing reliable predictions for heavy-ion collision phenomenology.

Future work could explore the implications of these findings for higher-dimensional flows, more realistic equations of state at larger baryon chemical potentials, and the transition from the early non-equilibrium phase to the hydrodynamic regime in heavy-ion collisions. Additionally, investigating the role of other transport coefficients and their interplay with thermal conductivity would provide a more complete picture of causal parameter space in relativistic heavy-ion collisions in the non-linear regime.

## ACKNOWLEDGMENTS

V.R. acknowledges the financial support from Anusandhan National Research Foundation (ANRF), India through Core Research Grant , CRG/2023/001309. V.R. also acknowledges Department of Atomic Energy (DAE), India for financial support.

### Appendix A: Matrix Elements of $A^{\mu a}_{\nu}$

Below, we list the non-zero components of  $A^{\mu a}_{\nu}$ , organized by equation index  $\mu$ , derivative index a, and fluid variable index  $\nu$ .

From Eq. (9):

$$A_n^{1t} = \cosh \rho,$$

$$A_n^{1x} = \sinh \rho,$$

$$A_\rho^{1t} = n \sinh \rho,$$

$$A_\rho^{1x} = n \cosh \rho.$$

From Eq. (10):

$$\begin{split} A_{\varepsilon}^{2t} &= \cosh \rho, \\ A_{\varepsilon}^{2x} &= \sinh \rho, \\ A_{\rho}^{2t} &= \varepsilon (1 + c_s^2) \sinh \rho + 2q \cosh \rho, \\ A_{\rho}^{2x} &= \varepsilon (1 + c_s^2) \cosh \rho + 2q \sinh \rho, \\ A_q^{2t} &= \sinh \rho, \\ A_q^{2x} &= \cosh \rho. \end{split}$$

From Eq. (11):

$$\begin{split} A_{\varepsilon}^{3t} &= c_s^2 \sinh \rho, \\ A_{\varepsilon}^{3x} &= c_s^2 \cosh \rho, \\ A_q^{3t} &= \cosh \rho, \\ A_q^{3x} &= \sinh \rho, \\ A_{\rho}^{3x} &= \sin h \rho, \\ A_{\rho}^{3t} &= \varepsilon (1 + c_s^2) \cosh \rho + 2q \sinh \rho, \\ A_{\rho}^{3x} &= \varepsilon (1 + c_s^2) \sinh \rho + 2q \cosh \rho. \end{split}$$

From Eq. (12):

$$\begin{split} A_n^{4t} &= -\frac{1}{n} \left( \sinh \rho - \frac{5\lambda q}{8\varepsilon c_s^2} \cosh \rho \right), \\ A_n^{4x} &= -\frac{1}{n} \left( \cosh \rho - \frac{5\lambda q}{8\varepsilon c_s^2} \sinh \rho \right), \\ A_\varepsilon^{4t} &= \frac{\sinh \rho}{\varepsilon} - \frac{10\lambda q}{8\varepsilon^2 c_s^2} \cosh \rho, \\ A_\varepsilon^{4x} &= \frac{\cosh \rho}{\varepsilon} - \frac{10\lambda q}{8\varepsilon^2 c_s^2} \sinh \rho, \\ A_q^{4t} &= \frac{5\lambda}{4\varepsilon c_s^2} \cosh \rho, \\ A_q^{4t} &= \frac{5\lambda}{4\varepsilon c_s^2} \cosh \rho, \\ A_\rho^{4t} &= \cosh \rho + \frac{5\lambda q}{8\varepsilon c_s^2} \sinh \rho, \\ A_\rho^{4t} &= \cosh \rho + \frac{5\lambda q}{8\varepsilon c_s^2} \cosh \rho, \\ A_\rho^{4x} &= \sinh \rho + \frac{5\lambda q}{8\varepsilon c_s^2} \cosh \rho. \end{split}$$

The source vector  $B^{\mu}$  collects the non-derivative terms from the system of equations. Below we list each component  $B^{\mu}$  corresponding to Eqs. (9)–(12).

$$B^{1} = 0,$$

$$B^{2} = 0,$$

$$B^{3} = 0,$$

$$B^{4} = \frac{3qn}{k\varepsilon}.$$

<sup>[1]</sup> W. Israel, Ann. Phys. (N.Y.) **100**, 310 (1976).

<sup>[2]</sup> W. Israel and J. M. Stewart, Ann. Phys. (N.Y.) 118, 341

- Press, 1987).
- [4] C. Eckart, Phys. Rev. 58, 919 (1940).
- [5] G. S. Denicol, H. Niemi, E. Molnar, and D. H. Rischke, Phys. Rev. D 85, 114047 (2012).
- [6] R. Baier, P. Romatschke, D. T. Son, A. O. Starinets, and M. A. Stephanov, J. High Energy Phys. 04, 100 (2008).
- [7] M. Bemfica, M. M. Disconzi, J. Noronha, and P. Kovtun, Phys. Rev. D 100, 104020 (2019).
- [8] A. Pandya, E. R. Most, and F. Pretorius, Phys. Rev. D 106, 123036 (2022).
- [9] F. S. Bemfica, M. M. Disconzi, and J. Noronha, Phys. Rev. X 12, 021044 (2022). arXiv:2009.11388.
- [10] D. Jou, J. Casas-Vázquez, and G. Lebon, Extended Irreversible Thermodynamics (Springer, 1996).
- [11] L. Rezzolla and O. Zanotti, "Relativistic Hydrodynamics," Oxford University Press, Oxford (2013), ISBN 978-0-19-852890-6.
- [12] Y. Aharonov, A. Komar and L. Susskind, Phys. Rev. 182, 1400 (1969).
- [13] E. Krotscheck and W. Kundt, Commun. Math. Phys. 60, 2 (1978).
- [14] L. Gavassino, M. Antonelli and B. Haskell, arXiv:2006.09843 [gr-qc] (2020).
- [15] L. Gavassino, Phys. Rev. D 111, no.10, 103011 (2025) doi:10.1103/PhysRevD.111.103011 [arXiv:2502.08740 [nucl-th]].
- [16] S. Floerchinger F. C. Grossi , JHEP 08, 186 (2018), arXiv:1711.06687v2 [nucl-th].
- [17] S. Pu, T. Koide, and D. H. Rischke, Phys. Rev. D 81, 114039 (2010). arXiv:0907.3906.
- [18] R. Biswas, S. Mitra and V. Roy, Phys. Lett. B 838, 137725 (2023) doi:10.1016/j.physletb.2023.137725 [arXiv:2211.11358 [nucl-th]].
- [19] R. Biswas, A. Dash, N. Haque, S. Pu and V. Roy, JHEP 10, 171 (2020) doi:10.1007/JHEP10(2020)171 [arXiv:2007.05431 [nucl-th]].
- [20] P. Romatschke, Int. J. Mod. Phys. E 19, 1 (2010).
- [21] J. Sammet, M. Mayer, and D. H. Rischke, Phys. Rev. D **107**, 114028 (2023). arXiv:2302.01070 DOI:10.1103/PhysRevD.107.114028
- [22] S. Bhattacharyya, S. Mitra and S. Roy, Phys. Lett. B 856, 138918 (2024) doi:10.1016/j.physletb.2024.138918 [arXiv:2407.18997 [nucl-th]].
- [23] M. Spaliński and B. Withers, Phys. Rev. D 109, 046018 (2024).
- [24] G. Perna and E. Calzetta, Phys. Rev. D 104, 096005 (2021). arXiv:2108.01114.
- [25] C. V. Brito and G. S. Denicol, Phys. Rev. D 105, 096026 (2022). arXiv:2107.10319.
- [26] F. S. Bemfica, M. M. Disconzi, and J. Noronha, Phys.

- Rev. Lett. 122, 221602 (2019). arXiv:1901.06701.
- [27] D.-L. Wang and S. Pu, Phys. Rev. D 109, L031504 (2024). arXiv:2309.11708.
- [28] W. A. Hiscock and L. Lindblom, Phys. Rev. D 31, 725 (1985).
- [29] L. Gavassino, Entropy 26, 147 (2024). arXiv:2312.13553 DOI:10.3390/e26020147
- [30] W. A. Hiscock and L. Lindblom, Phys. Lett. A 131, 509 (1988).
- [31] P. Danielewicz and M. Gyulassy, Dissipative phenomena in quark-gluon plasmas, Phys. Rev. D **31**, 53 (1985).
- [32] C. Eckart, The Thermodynamics of Irreversible Processes. III. Relativistic Theory of the Simple Fluid, Phys. Rev. 58, 919 (1940).
- [33] T. Kunihiro and K. Tsumura, Stable first-order particleframe relativistic hydrodynamics for dissipative systems, Phys. Lett. B 668, 425 (2008).
- [34] A. Monnai, Landau and Eckart frames for relativistic fluids in nuclear collisions, Phys. Rev. C 100, 014901 (2019)
- [35] J. I. Kapusta and C. Gale, Finite-Temperature Field Theory: Principles and Applications, 2nd ed. (Cambridge University Press, Cambridge, 2006).
- [36] S. Weinberg, Gravitation and Cosmology: Principles and Applications of the General Theory of Relativity (John Wiley & Sons, New York, 1972).
- [37] P. F. Bedaque and A. W. Steiner, Phys. Rev. Lett. 114, 031103 (2015).
- [38] S. Borsányi, Z. Fodor, C. Hoelbling, S. D. Katz, S. Krieg, and K. K. Szabó, Phys. Lett. B 730, 99 (2014). arXiv:1309.5258 DOI:10.1016/j.physletb.2014.01.007
- [39] S. Chakrabarty, Transport coefficients of quark-gluon plasma, Pramana 25, 673 (1985).
- [40] S. Mitra and V. Chandra, Phys. Rev. D 96, no.9, 094003 (2017) doi:10.1103/PhysRevD.96.094003 [arXiv:1702.05728 [nucl-th]].
- [41] G. Kadam, H. Mishra, and L. Thakur, Electrical and thermal conductivities of hot and dense hadronic matter, Phys. Rev. D 98, 114001 (2018).
- [42] M. Greif, F. Reining, I. Bouras, G. S. Denicol, Z. Xu and C. Greiner, Phys. Rev. E 87, 033019 (2013) doi:10.1103/PhysRevE.87.033019 [arXiv:1301.1190 [hep-ph]].
- [43] R. Marty, E. Bratkovskaya, W. Cassing, J. Aichelin and H. Berrehrah, Phys. Rev. C 88, 045204 (2013) doi:10.1103/PhysRevC.88.045204 [arXiv:1305.7180 [hepph]].
- [44] P. Romatschke, Int. J. Mod. Phys. E 19, 1 (2010). arXiv:0902.3663.
- [45] C. Plumberg et al., Phys. Rev. C 105, L061901 (2022). arXiv:2103.15889.